Nuclear Engineering and Technology 53 (2021) 509–521

Contents lists available at ScienceDirect

Nuclear Engineering and Technology

journal homepage: www.elsevier.com/locate/net

Original Article

Preliminary analyses on decontamination factors during pool scrubbing with bubble size distributions obtained from EPRI experiments

Yoonhee Lee [a, *], Yong Jin Cho [a], Inchul Ryu [b]

[a] Department of Nuclear Safety Research, Korea Institute of Nuclear Safety, 62 Gwahak-ro, Yuseong-gu, Daejeon, 34142, Republic of Korea
[b] PSA& PSR Business Group, Level 2 Probabilistic Risk Assessment, KEPCO Engineering & Construction Company Inc., 269 Hyeoksin-ro, Gimcheon-si, Gyeongsangbuk-do, 39660, Republic of Korea

ARTICLE INFO

Article history:
Received 3 June 2020
Received in revised form
10 August 2020
Accepted 12 August 2020
Available online 23 August 2020

Keywords:
Severe accident
Pool scrubbing
Size distribution of bubbles
Decontamination factor
LACE-ESPAÑA
SPARC-90
I-COSTA

ABSTRACT

In this paper, from a review of the size distribution of the bubbles during pool scrubbing obtained from experiments by EPRI, we apply the bubble size distributions to analyses on the decontamination factors of pool scrubbing via I-COSTA (In-Containment Source Term Analysis). We perform sensitivity studies of the bubble size on the various mechanisms of deposition of aerosol particles in pool scrubbing. We also perform sensitivity studies on the size distributions of the bubbles depending on the diameters at the nozzle exit, the molecular weights of non-condensable gases in the carrier gases, and the steam fractions of the carrier gases. We then perform analyses of LACE-ESPAÑA experiments and compare the numerical results to those from SPARC-90 and experimental results in order to show the effect of the bubble size distributions.

1. Introduction

Pool scrubbing refers to the removal of aerosol particles in gas bubbles rising in a water pool. In this phenomenon, the pool plays a role of a filter. Pool scrubbing is a very relevant issue in nuclear safety [1–4], since it is a key phenomenon to reduce the amount of fission product release to the environment during severe accidents. Pressure suppression pool and wet well are such pools in Boiling Water Reactors (BWRs) although they are preliminarily designed to avoid over pressurization of the wetwell space [1]. Pool scrubbing is not limited to BWRs; it can also occur in Pressurized Water Reactors (PWRs), i.e., release of radioactivity through safety injection piping directly into a tank containing water located in the auxiliary building. In corium concrete interaction, which causes release of semi- and low-volatile fission products as well as production of large amounts of concrete aerosols, pool scrubbing would also occur if the corium is overlaid by a water pool with a certain height [1,2].

The main phenomena influencing the retention of the fission products when bubbles rise during pool scrubbing are centrifugal deposition, diffusion, and settling [1,5–7]. Centrifugal deposition of the fission products occurs as bubbles larger than a critical size experience surface circulation as they rise through the liquid, i.e., the bubbles rotates due to surrounding water. A peripheral velocity then induces a centrifugal force on the particles in the gas located near the bubble wall. Diffusion of the aerosol particles within the bubbles is a result of Brownian motion caused by the stochastic nature of gas molecule collisions with the particles. Settling occurs by gravitational force within the bubbles. The process of fission product retention depends on the depth of the water pool, the size and shape of the bubbles, the size of the aerosol particles, and properties of the liquid phase and gas phase. The amount of fission products released from the aforementioned pool scrubbing process is expressed by the decontamination factor, which is defined as the ratio of the mass of fission products entering the water pool volume to the mass released from the surface of the pool.

Based on the results of EPRI experiments [8,9], especially on the bubble hydrodynamics, computer codes such as SPARC-90 [10],

* Corresponding author.
E-mail address: yooney@kins.re.kr (Y. Lee).

https://doi.org/10.1016/j.net.2020.08.013

Nomenclature

ab_j	aspect ratio of bubble with φ_j
A_j	surface area of bubble with φ_j
a_j	length of major axis of bubble with φ_j
b_j	length of minor axis of bubble with φ_j
c_j	$(a_j^2 - b_j^2)^{1/2}$
c_l	heat capacity of liquid water (J/g/K)
Cn_i	Cunningham slip correction factor for aerosol particle with d_i
c_s	heat capacity of solid (J/g/K)
$C_{v,nc}$	heat capacity of non-condensable gas at constant volume (J/g-mole/K)
$C_{v,vap}$	heat capacity of water vapor at constant volume (J/g-mole/K)
$D(d_i)$	diffusion coefficient for aerosol particle with equivalent diameter of d_i
DF_{br}	decontamination factor during bubble rise
$D_g(x)$	equivalent diameter of globule at a depth of x
$D_{g,ini}$	equivalent diameter of the globule at the nozzle exit
DF_k	decontamination factor in zone k
$DF(\varphi_j, d_i)$	functionalized decontamination factor for aerosol particle with d_i and bubble with φ_j
d_i	average equivalent diameter of the aerosol particle in section i
dQ_j	heat added to bubble of φ_j
dW_j	work of expansion done by bubble with φ_j from pressure drop, vapor production, and temperature change
dx	unit distance of bubble rise
$E_{c1}(j)$	eccentricity of bubble with φ_j
$E_{c2,j}$	$\sin^{-1}E_{c1,j}$
g	gravitational acceleration constant
i	section index on the size distribution of the aerosol particles
IMP_k	importance of the decontamination factor in zone k
j	section index on the size distribution of the bubbles
k	zone index (injection zone, transition zone, and bubble rise zone)
k_B	Boltzmann's constant
$M_{Fr}(d_i)$	mass fraction of aerosol particles with d_i
$m_{l,j}$	mass of condensed water on the surface aerosol particles in bubbles of φ_j
$M_{nc,j}$	g-moles of non-condensable gas in bubbles of φ_j
$m_{s,j}$	mass of solid as aerosol particles in bubbles of φ_j
$M_{vap,j}$	g-moles of vapor in bubble of φ_j
$M_{t,j}$	total g-moles of vapor and non-condensable gas in the of bubble of φ_j at x
$N_{Fr}(\varphi_j)$	number fraction of bubbles with φ_j
p	index of moving surface on bubbles
$P(x)$	pressure of the pool at x
$r_{c,j}$	surface radius of curvature of bubbles with φ_j
$r_j(\theta)$	radial coordinate of bubbles with φ_j with θ
T	temperature of the carrier gas
$t_{b,j}$	rise time of bubble with φ_j
$t_e(\varphi_j, \theta)$	exposure time of the surface of a bubble with φ_j moving between $\theta_{j,p}$ and $\theta_{j,p+1}$
$T_j^*(x + dx)$	temperatures of bubbles with φ_j
$T_j^{**}(x + dx)$	temperatures of bubbles with φ_j; refer to Eq. (24)
$U_j(x)$	internal energy of bubble of φ_j
$U_j(x + dx)$	internal energy of bubble of φ_j at $x + dx$, considering first law of thermodynamics; refer to Eq. (21)
$U_j^*(x + dx)$	internal energy of bubble of φ_j at $x + dx$, calculated by considering thermodynamic state of the bubbles; refer to Eq. (23)
$v_B(\varphi_j, \theta, d_i)$	local deposition velocity of aerosol particles with d_i in a bubble of φ_j
$v_c(\varphi_j, \theta, d_i)$	centrifugal deposition velocity of aerosol particles with d_i on the local surface θ of a bubble with equivalent diameter of φ_j
$v_g(d_i)$	gravitational settling velocity of aerosol particle with equivalent diameter of d_i
$v_n(\varphi_j, \theta, d_i)$	net deposition velocity of aerosol particle having equivalent diameter of d_i, on the local surface θ of a bubble with φ_j
$v_r(\varphi_j)$	rise velocity of bubbles with φ_j
$v_s(\varphi_j, \theta)$	local surface velocity on the surface θ of bubble with φ_j
$v_v(\varphi_j)$	vapor velocity of a bubble with φ_j
x	distance from the nozzle exit
θ	cylindrical polar coordinate on the local surface of a bubble ($-\pi/2 \leq \theta \leq \pi/2$)
$\theta_{j,p}$	discretized cylindrical polar coordinates on the local surface of a bubble with φ_j
λ_{vap}:	internal energy of evaporation at 273.15 K, 1 atm (J/g-mole)
μ	viscosity of carrier gas
ρ_p	pool liquid density
σ	standard deviation of the bubble size distribution
φ_j	average equivalent diameter of bubbles in section j
$\overline{\varphi}$	average diameter of the bubble size distribution

BUSCA [11], MELCOR [12], etc. were developed to analyze the pool scrubbing phenomena and accident scenarios related with pool scrubbing. The aforementioned codes have been validated with numerous experimental results on decontamination factors during pool scrubbing, such as LACE-ESPAÑA [13], POSEIDON [14], ACE [5], PASSAM [15], etc. With the aforementioned computer codes, comparative studies on modeling of the pool scrubbing and sensitivity analyses [5,6] have been performed for the various factors affecting the calculation of decontamination factors, such as bubble size, submergence depth, size of the aerosol particles, etc. One of the main conclusions of these studies is that the equivalent diameter of the bubble, obtained by calculating the diameter of a sphere having the same volume as a single bubble [8], is one of the most critical points for the calculation of the decontamination factors.

In the conventional computer codes for pool scrubbing, the average equivalent diameter of the bubble is considered when analyzing bubble dynamics and behavior of the fission products in the bubble and to calculate the decontamination factors. According to Ref. [6], the average equivalent diameter has been selected to provide conservative results on the decontamination factors in the conventional computer codes. However, the results of EPRI experiments [9] show bubbles during pool scrubbing have size distributions. Depending on the size of the bubbles, there are differences in their local surface velocity, which leads to differences in centrifugal deposition velocities, deposition velocities due to Brownian diffusion, gravitational settling velocities, etc. Net deposition velocities calculated from the aforementioned various mechanisms of retention also depend on the size of the bubbles and it leads to bubble-size-dependent decontamination factors.

In addition, in accordance with legislation on severe accidents in Korea, there is a quantitative safety goal of new and/or operating nuclear power plants in terms of the amount of radioactive materials released and this goal should be evaluated by a best-estimate methodology in the analyses of severe accidents [16]. The pool scrubbing phenomenon is known as one of the most important phenomena to evaluate the aforementioned safety goal. The computer codes for the pool scrubbing, however, have been developed to be as conservative as possible; for example, MELCOR [12] uses 0.7 cm as a default value for the average equivalent diameter of the bubbles to provide conservative decontamination factors [5]. Considering the legislation on the severe accidents in Korea, it is now important to analyze the degree of conservatism provided by conventional pool scrubbing codes in a quantitative manner and to propose a methodology that is closer to best-estimate methodology. We would like to propose such a methodology by considering size distributions of the bubbles during pool scrubbing.

In this paper, first, we review the size distributions of the bubbles during pool scrubbing and obtain the discretized size distribution. We then propose a calculational procedure for the decontamination factors in order to consider bubble size distributions. The procedure is based on the bubble-size-dependent velocities of centrifugal deposition, Brownian diffusion, and gravitational settling, and the derived net deposition velocities from the aforementioned retention mechanisms. The procedure is coupled with analysis modules of the bubble-hydrodynamics, bubble-thermodynamics, and change of aerosol size due to hygroscopic growth, which are based on the module used in SPARC-90. The coupled modules are implemented in an in-house code named I-COSTA (In-COntainment Source Term Analysis).

Second, we perform sensitivity analyses of bubble sizes on the aforementioned various deposition velocities to find the most dominant mechanism of the aerosol particle retention as a function of the equivalent diameters of the bubbles. We also perform sensitivity studies on the size distributions of the bubbles depending on the diameters at the nozzle exit, the molecular weights of non-condensable gases in the carrier gases, and the steam fractions of the carrier gases. We subsequently apply I-COSTA to analyses of LACE-ESPAÑA experiments [13] and compare the numerical results to those from SPARC-90 [10] and experimental results. In the comparison, we perform the calculations by SPARC-90 for two cases: one with default sensitivity coefficients for the average equivalent diameter of the bubbles and the other using the average equivalent diameter obtained by averaging bubble size distributions in EPRI experiments; i.e., the average equivalent diameter is the same as that of the distribution used in I-COSTA. Modification of the average equivalent diameter of the bubbles is done by changing the sensitivity coefficients on the bubble size in order to show the effect of the distribution itself on calculating the decontamination factor.

This paper is organized as follows. Section 2 provides a brief description of the characteristics of the distribution of the bubble size obtained from EPRI experiments [8,9] and the calculation of the discretized size distribution of the bubbles for numerical analyses. In Section 3, we describe the calculational method of the bubble-size-dependent decontamination factors when bubbles rise in the pool. Section 4 provides results of sensitivity analyses on the various mechanisms of aerosol retention in order to show the most dominant mechanism as the bubble size changes. This Section presents the results of sensitivity studies on the size distributions of the bubbles, depending on the diameters at the nozzle exit, the molecular weights of non-condensable gases in the carrier gases, and the steam fractions of the carrier gases. In Section 5, the numerical results of the application to LACE-ESPAÑA experiments are explained. The importance of the decontamination factor in the various zones, i.e., the injection zone, the transition zone where globule breakup occurs since the globule is unstable, and the bubble rise zone where the ultimate size distribution of the bubbles is achieved according to the Weber number, is also explained in this Section. Finally, a discussion and conclusions are provided in Section 6.

2. Bubble size distributions during bubble rise in pool scrubbing

2.1. Review on the size distributions obtained from EPRI experiment

Numerous experiments have been performed on the measurement of the bubble size distributions in a two-phase flow. However, if we focus on the bubble size distributions during pool scrubbing, where aerosol particles carried by non-condensable gases are mixed with the steam and they are injected into the stagnant pool, there are few experiments that we can refer to. The EPRI experiment [8] is one of the most valuable experiments and has been widely used for the development and validation of the conventional computer codes for bubble hydrodynamics during pool scrubbing, e.g., SPARC-90 [10], BUSCA [11], MELCOR [12], etc. It was performed on the formation of globules at the nozzle and on the breakup of the globules into bubbles rising in a one-dimensional (axial) direction. Most of the correlations and the sensitivity coefficients used in the conventional computer codes are based on the results of the EPRI experiment [8]. However, as discussed in the previous Section, most of the conventional computer codes have used the average equivalent diameter of the bubbles only, even though the size distributions and the average diameters of the bubbles were measured simultaneously in the experiments. Considering the purpose of the experiment and consistency with the correlations and the sensitivity coefficients used in I-COSTA, which is developed based on SPARC-90 [10], we are going to use the size distributions of the bubbles measured in the EPRI experiment for more realistic analyses on the pool scrubbing.

According to the experiment, the initial globule formed during injection is unstable. Breakup of the initial globule begins almost immediately after it leaves the injection zone. As the globule rises in the water pool, it breaks up into smaller bubbles until an ultimate size distribution of the bubbles is made, where the Weber number of the globule is less than 15. Based on the visualization studies by EPRI, the breakup length, which is required to reach the ultimate size distribution, corresponds to approximately ten times the initial globule diameter from the nozzle outlet. After the ultimate size distribution is made, the bubble column does not remain static; instead, the bubbles break up and coalesce continuously such that the net effect is that there is no change in the size distribution of the bubbles.

From the photographs taken during the experiments by EPRI [8], most of the bubbles have an ellipsoid shape. Therefore, the size of the bubbles is determined by measuring the length of the major and minor axes of the ellipsoid representing the shape of the bubbles. The typical size distribution of bubbles is shown in Fig. 1: an average diameter of 5.64 mm and a logarithmic standard deviation (σ of 0.172. In this distribution, bubbles having an equivalent diameter greater than 13 mm account for less than 3%. Note that the continuous distribution in Fig. 1 is fitted by considering a large number of results in the experiments, i.e., it is a generalization of all experimental results.

EPRI performed several sensitivity studies on the bubble size distribution. First, as shown in Table 1, diameters of the nozzle exit do not have any effect on the ultimate size distribution of the bubbles since the breakup of the globule continues until the bubbles reach a stable size. Second, as shown in Table 2, the molecular

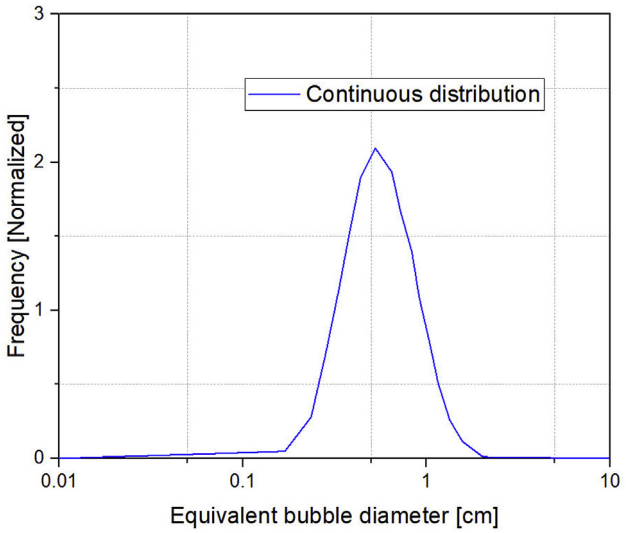

Fig. 1. Typical size distribution of the bubbles during pool scrubbing(Re-drawn figure from Ref. 7).

weight of the non-condensable gas in the carrier gas has little effect on the ultimate size distribution of the bubbles. The cause of the results is that the stability of the bubbles affecting the size distributions is determined by the density of the continuous phase and the surface tension of the liquid-gas interface, which is consistent with the definition of the Weber number indicating stability of the bubbles. In the experiments, water was always a continuous phase and the surface tensions of the interfaces between water-air, water-helium, and water-hydrogen were all nearly equal in magnitude [8].

EPRI also performed sensitivity studies on the steam fractions. As shown in Table 3, the mean equivalent diameters of the bubbles asymptotically approach the value of 5.6 mm, obtained using pure non-condensable gases shown in Figs. 2 and 3 at low steam fractions. As the steam fraction increases, the average equivalent diameter of the bubbles slowly decreases. When the fraction is 1.0, i.e., all steam is injected into the water pool, complete condensation is observed to occur within two initial globule diameters of the injector outlet. This indicates that most of the steam is condensing before the globule completely breaks up into small bubbles.

The bubble size distribution considered in this study is valid when the Weber number at the nozzle exit is less than 1E+05, with the diameters of the nozzle exit in a range between 10 mm and 20 mm, molecular weights of the non-condensable gases, and steam fractions in the carrier gases discussed in this Section. The range of the validity is consistent with those of the conventional computer codes such as SPARC-90 [10], BUSCA [11], MELCOR [12], etc.

2.2. Discretization of bubble size distribution for numerical analyses

In order to consider the size distribution of the bubbles in the calculations of decontamination factors, the continuous size of bubbles should be discretized into several sections, since it is difficult to consider a continuous distribution in the numerical method based on the discretization nature. In this study, the discretization is performed by integrating the continuous distribution on the bubble size over several numbers of sections on the size. This is expressed as Eq. (1). Note that the continuous distributions are fitted to a lognormal function in the EPRI report.

$$N_{Fr}(\overline{\varphi}_j) = \int_{\varphi_j}^{\varphi_{j+1}} \frac{1}{x\sigma\sqrt{2\pi}} \cdot \exp\left(\frac{-\{\ln(x) - \overline{\varphi}\}^2}{2\sigma^2}\right) dx, \quad (1)$$

where

φ_j, φ_{j+1} : minimum and maximum diameters of the bubbles in section j,
$\overline{\varphi}_j$: average equivalent diameter of the bubbles in section j,
$\overline{\varphi}$: average diameter of the bubbles in the distribution,
σ: standard deviation of the bubbles,
$N_{Fr}(\overline{\varphi}_j)$: number fraction of bubbles with $\overline{\varphi}_j$.

The discretized size distribution of the bubbles for seven sections, obtained from the continuous size distribution in Fig. 1, is shown in Fig. 2.

3. Calculation of bubble-size-dependent decontamination factors during bubble rise in pool scrubbing

In this study, since most of the computer codes on pool scrubbing are based on the experimental data obtained in the globular injection regime, i.e., the Weber number at the nozzle exit is less than 1E+05, we also focus on pool scrubbing in the globular regime. The models used in I-COSTA to analyze the aerosol retention at the nozzle exit, e.g., steam condensation, inertial impaction, etc., are the same as those used in SPARC-90 [10]. The empirical models in I-COSTA are based on the models used in SPARC-90 with slight modification to calculate the Weber number, void fraction, etc. The modified models were validated against results of RSE experiments [17]. In the following Sections, we describe the calculation of the centrifugal deposition velocity, the deposition velocities due to Brownian diffusion and gravitational settling, and the decontamination factors calculated from the aforementioned various deposition velocities, which are functionalized over the size of bubbles during bubble rise. We also describe the calculational

Table 1
Comparison of average equivalent diameter and standard deviation of the bubbles (Sensitivity on the diameters of nozzle exit).

		Avg. [cm]	log (σ)
Typical distribution(Nozzle diameter 9.9E-03 m)		0.564	0.172
Nozzle diameter	1.27E-02 m	0.554	0.199
	2.02E-02 m	0.589	0.191

Table 2
Comparison of average equivalent diameter and standard deviation of the bubbles (Sensitivity on the molecular weights of non-condensable gases).

		Avg. [cm]	log (σ)
Typical distribution(Nitrogen)		0.564	0.172
Molecular weight	Hydrogen	0.562	0.193
	Helium	0.466	0.200

Table 3
Comparison of average equivalent diameter and standard deviation of the bubbles (Sensitivity on the steam fractions in the carrier gases).

		Avg. [cm]	log (σ)
Typical distribution(0.07)		0.564	0.172
Steam fraction	0.25	0.578	0.181
	0.50	0.545	0.183
	0.75	0.467	0.189
	0.95	0.361	0.163

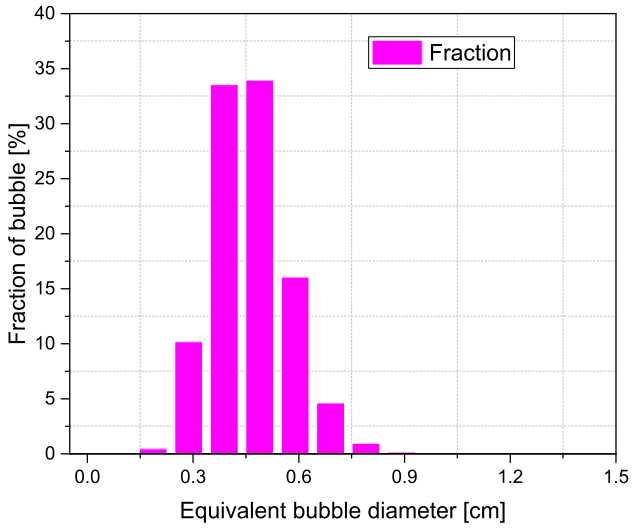

Fig. 2. Discretized distribution obtained from the continuous typical size distribution of the bubbles during pool scrubbing.

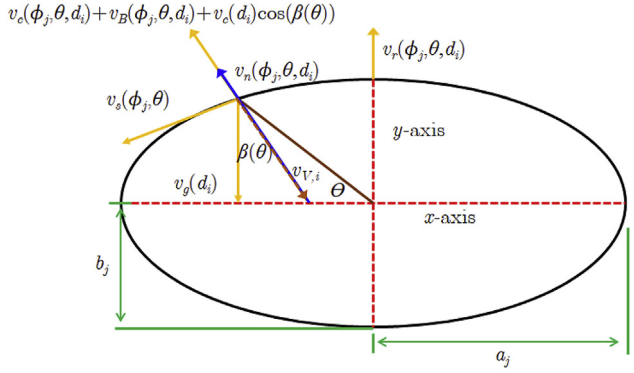

Fig. 3. Rising bubble with various retention mechanisms of aerosol particles.

procedure for the bubble-size-dependent decontamination factors coupled with the bubble-hydrodynamics, the bubble-thermodynamics, and the change of aerosol particle diameters due to hygroscopic growth.

3.1. Functionalization of decontamination factor on the size of bubbles during bubble rise

As mentioned in Section 1, the decontamination factors during bubble rise are determined by the centrifugal deposition, Brownian diffusion, and gravitational settling. By the Stokes law, the gravitational settling velocity, $v_g\,(d_i)$, is expressed as

$$v_g(d_i) = \frac{1}{18\mu}\rho_p \cdot d_i^2 \cdot g \cdot Cn_i, \tag{2}$$

d_i: equivalent diameter of aerosol particle in section i,
Cn_i: Cunningham slip correction factor for aerosol particle with d_i,
μ: viscosity of carrier gas,
ρ_p: pool liquid density,
g: gravitational acceleration constant.

The centrifugal deposition occurs due to surface circulation as the bubbles rise through the liquid surface when the size of the bubble is greater than the critical size [10,[18]], i.e., the bubbles rotates due to surrounding water at velocity of $v_s(\varphi_j, \theta)$. The centrifugal deposition velocity of the aerosol particles with an equivalent diameter of d_i on the local surface θ of the bubble with an equivalent diameter of φ_j, $v_c(\varphi_j, \theta, d_i)$, is expressed as follows:

$$v_c(\varphi_j,\theta,d_i) = \frac{v_s^2(\varphi_j,\theta)v_g(d_i)}{r_c(\varphi_j,\theta)g}\ , \tag{3}$$

where

φ_j: equivalent diameter of the bubbles in section j,
θ: cylindrical polar coordinate on the local surface of the bubble ($-\pi/2 \le \theta \le \pi/2$),
$v_s(\varphi_j, \theta)$: local surface velocity on the surface θ of bubble with φ_j, calculated as

$$v_s(\varphi_j,\theta) = v_r(\varphi_j)\left\{\frac{1}{E_{c2}}\left(1-\frac{b_j}{c_j}\tan\left(\frac{c_j}{b_j}\right)\right) - v_r(\varphi_j)\frac{b_j}{c_j}\right\}\frac{r_j\cos\theta}{a_j}\left\{\left(\frac{b_j}{c_j}\right)^2+\left(\frac{r_j\sin\theta}{b_j}\right)^2\right\}^{-1/2}, \tag{4}$$

$v_r\,(\varphi_j)$: rise velocity of bubbles with φ_j, calculated by the correlations suggested on Ref. [19], which are based on the data from Ref. [10,12,20]:

$$v_r(\varphi_j) = \begin{cases} 7.876\cdot\left(\dfrac{\gamma_p}{\rho_p}\right)^{1/4} & (\text{for } \varphi_j \le 0.5\ cm) \\ 1.40713\cdot 7.876\cdot\left(\dfrac{\gamma_p}{\rho_p}\right)^{1/4}\cdot\varphi_j^{0.49275} & (\text{for } \varphi_j > 0.5\ cm) \end{cases}, \tag{5}$$

a_j: length of major axis of the bubbles with φ_j, calculated as follows:

$$a_j = \left\{\frac{3ab_j}{4\pi}\left(\frac{\pi}{6}\varphi_j\right)^3\right\}^{1/3} \tag{6}$$

ab_j: aspect ratio of bubbles with φ_j, calculated as follows [8,10,12]:

$$ab_j = \frac{a_j}{b_j} = 0.84107 + 1.13466 \cdot \varphi_j - 0.37950 \cdot \varphi_j^2, \tag{7}$$

b_j: length of minor axis of bubbles with φ_j,

$$c_j = \left(a_j^2 - b_j^2\right)^{1/2}, \tag{8}$$

$r_j(\theta)$: radial coordinate of bubbles with φ_j with θ, defined as

$$r_j(\theta) = \left(\left(\frac{\cos\theta}{b_j}\right)^2 + \left(\frac{\sin\theta}{a_j}\right)^2\right)^{-1/2}, \tag{9}$$

$E_{c1}(j)$: eccentricity of bubble with φ_j, defined as

$$E_{c1,j} = \left\{1 - \left(\frac{b_j}{a_j}\right)^2\right\}^{1/2}, \tag{10}$$

$$E_{c2,j} = \sin^{-1} E_{c1,j}, \tag{11}$$

$r_{c,j}$: surface radius of curvature of bubble with φ_j, defined as

$$r_{c,j} = c_j \left\{\left(\frac{b_j}{c_j}\right)^2 + \left(\frac{r_j \sin\theta}{b_j}\right)^2\right\}^{3/2} \cdot \left(\frac{b_j}{c_j} + \frac{a_j}{c_j}\right)^{-1}, \tag{12}$$

Deposition due to Brownian diffusion is done by diffusion of aerosol particles within a bubble. The diffusion coefficient for the aerosol particles with an equivalent diameter of d_i, $D(d_i)$, can be calculated with the Stokes-Einstein equation [10,21] as follows:

$$D(d_i) = \frac{k_B T C n_i}{\pi d_i \mu}, \tag{13}$$

where

k_B: Boltzmann's constant,
T: temperature of the carrier gas.

With Eq. (13), the local deposition velocity of the aerosol particles with d_i in the bubble of φ_j due to Brownian diffusion, $v_B(\varphi_j, \theta, d_i)$, can be calculated from penetration theory of mass transfer [10,22,23]:

$$v_B(\varphi_j, \theta, d_i) = \left(\frac{D(d_i)}{\pi t_e(\varphi_j, \theta)}\right)^{1/2}, \tag{14}$$

where
$t_e(\varphi_j, \theta)$: exposure time of the surface of the bubble with φ_j moving between $\theta_{j,k}$ and $\theta_{j,k+1}$, calculated as the following equation:

$$t_e(\varphi_j, \theta) = \frac{\left[\{r_j(\theta)\cos\theta_{j,p+1} - r_j(\theta)\cos\theta_{j,p}\}^2 - \{r_j(\theta)\sin\theta_{j,p+1} - r_j(\theta)\sin\theta_{j,p}\}^2\right]^{1/2}}{v_s(\varphi_j, \theta)}, \tag{15}$$

$\theta_{j,k}$: discretized cylindrical polar coordinates on the local surface of a bubble with φ_j satisfying:

$$\theta_{j,p} \le \theta < \theta_{j,p+1}, \quad \text{and} \quad -\pi/2 \le \theta_{j,p} < \theta_{j,p+1} \le \pi/2. \tag{16}$$

With Eqs. (2)~(16) and the vapor velocity $v_v(\varphi_j)$, the net deposition velocity of an aerosol particle having an equivalent diameter of d_i, on the local surface θ of a bubble with φ_j, $v_n(\varphi_j, \theta, d_i)$ is expressed as

$$v_n(\varphi_j, \theta, d_i) = v_c(\varphi_j, \theta, d_i) + v_B(\varphi_j, \theta, d_i) + v_g(d_i) \cdot \cos\beta(\theta) + v_v(\varphi_j), \tag{17}$$

and the relationship between each mechanism of retention is shown in Fig. 3.

Eq. (17) can be used to calculate the decontamination factor of the aerosol particle with d_i, captured by the three aforementioned retention mechanisms, in the bubbles of φ_j. The decontamination factor, in this case, is the mass flow rate of the aerosol particles into the bubble divided by the mass flow rate of the particles out of the bubble. Therefore, the decontamination factor can be functionalized over the equivalent diameter of an aerosol particle, d_i, and the equivalent diameter of a bubble φ_j, as given in the following equation:

$$DF(\varphi_j, d_i) = \exp\left\{\frac{1}{\frac{4}{3}\pi {a_j}^2 b_j} \int_0^{t_{b,j}} \int_{A_j} v_{n,j}(\varphi_j, \theta, d_i) dA dt\right\}, \tag{18}$$

where

$t_{b,j}$: rise time of bubble with φ_j,
A_j: surface area of bubble with φ_j.

With Eq. (18), the decontamination factor during bubble rise can be calculated as follows:

$$DF_{br} = \frac{1}{\sum_j \sum_i \frac{N_{Fr}(\varphi_j) \cdot M_{Fr}(d_i)}{DF(\varphi_j, d_i)}}, \tag{19}$$

where

$M_{Fr}(d_i)$: mass fraction of aerosol particles with d_i, $\sum_i M_{Fr}(d_i) = 1$,
$N_{Fr}(\varphi_j)$: number fraction of bubbles with φ_j, $\sum_j N_{Fr}(\varphi_j) = 1$.

Note that the overall decontamination factor is obtained by the harmonic average of the distributed decontamination factor, in order to conserve the total amount of aerosol particles removed during pool scrubbing.

3.2. Calculational procedure for the bubble-size-dependent decontamination factors

In the calculation of the decontamination factor, bubble-hydrodynamics is required to calculate velocities and volume fractions of the globule and bubbles. Bubble thermodynamics is also required to calculate pressures and temperatures of bubbles, which are required to predict the change of size of aerosol particles due to hygroscopic growth. In I-COSTA, calculational modules of bubble-hydrodynamics and bubble-thermodynamics are based on those used in SPARC-90 [10] and MELCOR codes [12]. In this Section, we describe the calculational procedure of decontamination factors considering bubble-hydrodynamics and bubble-thermodynamics.

For the rise of a bubble from a depth of x to $x + dx$ and given the size distribution of the bubbles, the first step is to calculate the volume fractions of the globule and bubbles. This calculation is based on the experimental observation that the volume of the initial globule shows a linear decrease expressed as follows [10–12]:

$$D_g(x) = D_{g,ini}\left(1 - \frac{x}{12 \cdot D_{g,ini}}\right), \tag{20}$$

where

$D_g(x)$: equivalent diameter of globule at a depth of x,
$D_{g,ini}$: equivalent diameter of the globule at the nozzle exit.

If the volume fraction of the bubble is greater than zero, we assume that aerosol particles are deposited with a rise of dx. Then, for each section of bubbles, we make an initial guess on the temperatures of the bubbles with φ_j, $T_j^*(x + dx)$. With the temperatures, we calculate the saturation ratio and solve the Mason equation [24] to obtain the diameter of aerosol particles after hygroscopic growth in each section of the bubbles.

The next step is to calculate the internal energy of a bubble with consideration of the heat added to the bubble, the work of expansion in dx done by the bubble from pressure drop, vapor production, and temperature change. This is done by the following equation:

$$U_j(x + dx) = U_j(x) + dQ_j - dW_j, \tag{21}$$

where

$U_j(x + dx)$: internal energy of bubble of φ_j at $x + dx$.
$U_j(x)$: internal energy of bubble of φ_j at x,
dQ_j: heat added to bubble of φ_j,
dW_j: work of expansion done by the bubbles with φ_j from pressure drop, vapor production, and temperature change, calculated as

$$dW_j = R \cdot \left\{ M_{t,j} \cdot T_j^*(x) \cdot \ln\left(\frac{P(x)}{P(x+dx)}\right) + dM_{vap,j} \cdot T_j^*(x) \right\} + R \cdot \left\{ M_{vap,j} \cdot \left(T_j^*(x + dx) - T_j^*(x) \right) \right\}, \tag{22}$$

$P(x)$: pressure of the pool at x.
$M_{t,j}$: total g-moles of vapor and non-condensable gas in the bubble of φ_j.
$M_{vap,j}$: g-moles of vapor in the bubble of φ_j.
The internal energy can also be calculated by considering the thermodynamic state of the bubbles at $x + dx$ as follows:

$$U_j^*(x + dx) = M_{vap,j}\lambda_{vap} + \int_{273.15}^{T_j^*(x+dx)} \left(M_{vap,j}C_{v,vap} + M_{nc,j}C_{v,nc} + m_{l,j}c_l + m_{s,j}c_s \right) dT, \tag{23}$$

where

λ_{vap}: internal energy of evaporation at 273.15 K, 1 atm (J/g-mole),
$C_{v,vap}$: heat capacity of water vapor at constant volume (J/g-mole/K)
$M_{nc,j}$: g-moles of non-condensable gas in bubbles of φ_j,
$C_{v,nc}$: heat capacity of non-condensable gas at constant volume (J/g-mole/K)
$m_{l,j}$: mass of condensed water on the surface aerosol particles in bubbles of φ_j,
c_l : heat capacity of liquid water (J/g/K)
$m_{s,j}$: mass of solid aerosol particles in bubbles of φ_j
c_s : heat capacity of solid (J/g/K).

With Eqs. (21) and (23), we can obtain the updated temperature, $T_j^{**}(x + dx)$, as follows:

$$T_j^{**}(x + dx) = T_j^*(x + dx) + \frac{U_j(x + dx) - U_j^*(x + dx)}{M_{vap,j}C_{v,vap} + M_{nc,j}C_{v,nc} + m_{l,j}c_l + m_{s,j}c_s}. \tag{24}$$

$T_j^*(x + dx)$ is then replaced with $T_j^{**}(x + dx)$. The aforementioned procedures are repeated until $T_j^*(x + dx)$ is converged. After we obtain the converged $T_j^*(x + dx)$, the various deposition velocities explained in Section 3.1 are calculated to obtain the decontamination factors. In the calculation, the solutions of Mason equation, obtained by considering heat and mass transfer between the pool and the surface of the bubble, are also used. The calculational procedures are summarized in Fig. 4 and the algorithm is implemented in I-COSTA.

4. Sensitivity analyses on the mechanisms of aerosol retention and size distribution of the bubbles during pool scrubbing

In this Section, I-COSTA is applied to sensitivity analyses on the various mechanisms of aerosol retention and on the size distributions of the bubbles discussed in Section 2 during pool scrubbing. The geometric and thermophysical conditions of the pool are based

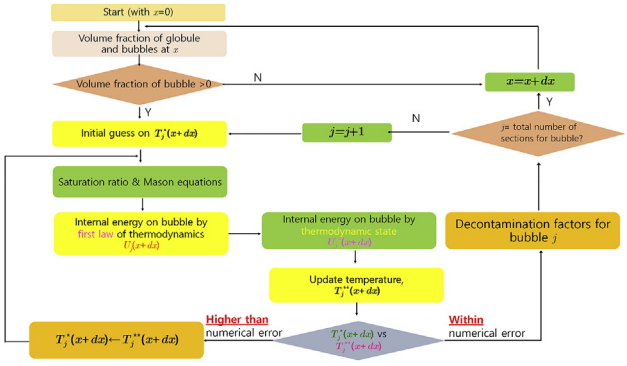

Fig. 4. Calculational procedure for bubble size-dependent decontamination factor.

on the RT-SB-12/13 test in LACE-ESPAÑA experiments [13]. The volume of the tank is 8.34 m^3 and it is filled with water. The depth of the pool is 3.0 m and the nozzle is installed in the horizontal direction with a submergence depth of 2.5 m. The region between the nozzle exit and the top of the pool where the globule and the bubbles rise is divided into 10 sub-regions. The length of each sub-region is 0.25 m. The aforementioned geometric and thermophysical conditions are summarized in Table 4.

4.1. Sensitivity studies on the mechanisms of aerosol retention

In the analyses, the area at the exit of the nozzle is 7.698E-07 m^2, which is equivalent to the exit diameter of the nozzle of 9.9E-04 m. CsI aerosol particles are considered in the studies since cesium (Cs) and iodine (I) are known to be the most important contributors to public risk [25] due to their relatively long half-life and high affinity to human organs. In addition, there is high potential to form small-sized aerosol particles in the case of CsI and they are relatively resistant to agglomeration and deposition [1]. We consider three cases for the size distribution of CsI, as shown in Table 5. The three cases are derived from the experimental conditions of LACE-ESPAÑA. Note that the range of the sizes of the aerosol particles in the experiment are based on analyses on the size of the aerosol particles in the containment during a severe accident. According to a survey of the literature [1,26–28], the size of aerosol particles during the severe accident is in the range of 5.0E-05–3.7E-04 cm with geometric standard deviation between 1.4–2.5 depending on the experimental conditions, i.e., experiments on the reactor coolant system, and those on the containment. Information on the aerosol particles and bubbles is summarized in Table 5. The net deposition velocities are compared with the deposition velocities according to the various retention mechanisms for the various bubble equivalent diameters in Fig. 5. Note that the number of discretized sections in the bubble size distributions is determined by sensitivity studies of the number of sections on the decontamination factors [25]. In addition, the velocities in Fig. 5 are average values considering the size distributions of the aerosol particles and the surfaces of the bubbles in cylindrical polar coordinates.

As shown in a. of Fig. 5, for the case of size 1, the net deposition velocity with bubble equivalent diameter of 0.01 cm is ~8.5E+02 cm/s in terms of normalized value and it decreases rapidly as the bubble equivalent diameter increases. The value is saturated at 0.5 cm/s when the bubble equivalent diameter is ~0.7 cm. For the other cases regarding the size of aerosol particles, i.e., sizes 2 and 3, trends in the changes of the net deposition velocities are similar, as shown in b and c of Fig. 5 and they are consistent with the change of the decontamination factor over the bubble equivalent diameter reported in Ref. [6].

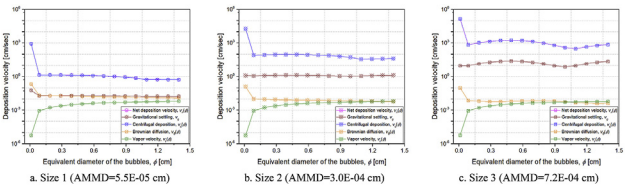

a. Size 1 (AMMD=5.5E-05 cm) b. Size 2 (AMMD=3.0E-04 cm) c. Size 3 (AMMD=7.2E-04 cm)

Fig. 5. Comparison of net deposition velocities to the deposition velocities of the various retention mechanisms for various sizes of the aerosol particles.

There is no large change in gravitational settling velocities as the bubble equivalent diameter changes for all cases of the aerosol sizes considered in this study since they are a function of the equivalent diameter of the aerosol particles only, as explained in Section 3. In the case of vapor velocities, they increase as the bubble equivalent diameter increases. In addition, regardless of the size of aerosol particles, the values of the vapor velocities are the same. The results are due to that the vapor velocities are proportional to steam flux transferring into the bubbles, and the amount of steam flux is proportional to the surface area of the bubbles.

In the case of deposition velocities due to Brownian diffusion, they decrease from 2.1E-01 cm/s to 9.6E-02 cm/s as the average mean mass diameter of aerosol particles increases from 5.5E-05 cm to 7.2E-04 cm. In addition, they decrease as the bubble equivalent diameter increases since they are inversely proportional to the exposure time of the moving surface, which is proportional to the bubble equivalent diameter, as shown in Eq. (15). However, they are not significant compared to the values of the centrifugal deposition velocities as shown in Fig. 5.

Centrifugal deposition velocities also decrease as the bubble equivalent diameter increases for all cases of the sizes of the aerosol

Table 4
Geometrical and thermophysical conditions of the pools in RT-SB-12/13 of LACE-ESPAÑA experiments.

Parameter		Value
Volume of the tank [m^3]		8.43
Water	Pressure [Bar]	1.9749
	Temperature [K]	382.62
Gas	Pressure [Bar]	2.280
	Temperature [K]	440.75
Pool depth [m]		3.0
Submersion depth [m]		2.5
Hole size at nozzle exit [m^2]		7.85398E-05
Computational conditions	Number of sub-regions for globule and bubble rise	10
	Number of sections for aerosol particles	10

Table 5
Information on the distribution of aerosol particles and bubbles.

Parameter		Value		
		Size 1	Size 2	Size 3
Aerosol type			CsI	
Aerosol	Avg. [cm]	5.5E-05	3.0E-04	7.2E-04
	Geometric Std.	1.6	2.3	1.6
	Injection rate [kg/sec]		5.0E-06	
Bubble	Avg. [cm]		0.564	
	Geometric Std.		0.172	

particles considered, since they are inversely proportional to the surface radius of the curvature for the bubble; i.e., they decrease as the bubble equivalent diameter decreases as the bubble equivalent diameter increases, as shown in Eq. (3).

From a comparison of the deposition velocities of the various retention mechanisms with the net deposition velocities, we find that the centrifugal deposition is the most dominant mechanism of the aerosol retention in the bubbles for the sizes of the aerosol particles in the containment during the severe accident. It is also the most sensitive mechanism to the change of the bubble equivalent diameters. Therefore, we can conclude that centrifugal deposition is the most important mechanism of retention in the calculation of the bubble-size-dependent decontamination factors.

Note that the equation on the centrifugal deposition velocity, Eq. (3), is derived assuming that there is no contaminant in the water, i.e., pure water. According to the work on Ref. [30], the rising velocity of the bubbles in the contaminated water is ~35% slower than that of the bubbles in pure water, which could result in slower centrifugal velocity, and hence the deposition rate will be slower. This effect will be studied as future work.

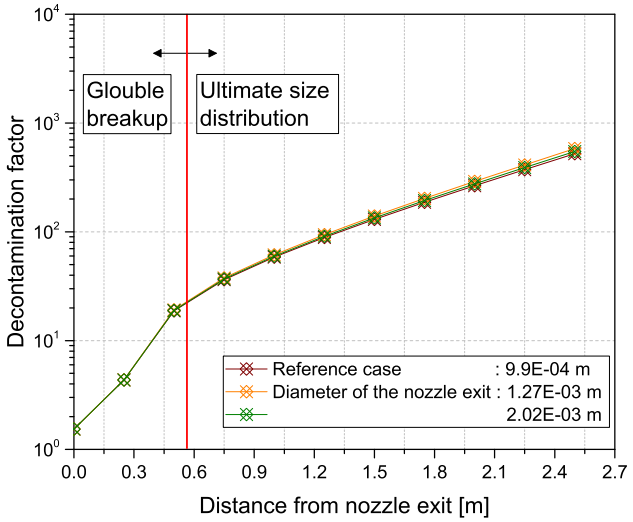

Fig. 6. Comparison of the decontamination factors for various diameters of the nozzle exit.

4.2. Sensitivity studies on the bubble size distributions

In the analyses, we perform sensitivity studies on various size distributions of the bubble. We consider three cases: effect of diameter at the nozzle exit (Case 1), effect of molecular weight of non-condensable gas (Case 2), and effect of steam fraction (Case 3). Similarly to the sensitivity studies in the previous Section, CsI aerosol particles with average diameter of 3.0E-04 cm and geometric standard deviation of 2.3 are injected at a rate of 5.0E-06 kg/s. The decontamination factors in the three cases are compared to the reference case in which the typical size distribution of the bubbles discussed in Section 2 is used. The average equivalent diameters and the geometric standard deviations for the three cases are listed in Table 6. Changes of decontamination factors according to the distance from the nozzle exit for the three cases are shown in Fig. 6–8, and the cumulative decontamination factors of the three cases for the entire processes are compared in Table 6.

For Cases 1 and 2, as shown in Figs. 6 and 7, and Table 6, the differences in the change of decontamination factors as the bubbles rise are less than 40% compared to those in the reference case. These results are attributed to the small effect that the nozzle diameters and the molecular weight of non-condensable gases respectively have on the ultimate size distributions of the bubbles, as explained in Section 2.

For Case 3, as shown in Fig. 8, when the steam fraction is lower than 0.95, the differences in the change of decontamination factors as the bubbles rise are less than 40% compared to those in the reference case. However, as the steam fraction increases to 0.95, the differences in the change of decontamination factors as the bubbles rise become 680% compared to those in the reference case. These results are ascribed to the small effect of the low steam fractions on the ultimate size distributions of the bubbles; however, the bubble

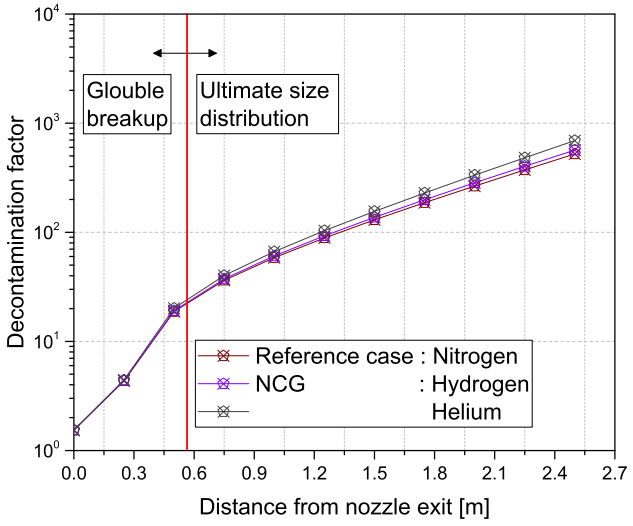

Fig. 7. Comparison of the decontamination factors for various molecular weights of the non-condensable gases.

Table 6
Comparison of overall decontamination factors for sensitivity studies on the size distributions of the bubbles.

Parameter		Value	
		DF	RCR*
Reference case (9.9E-04 m, Nitrogen, 0.07)	5.217e+02	1	
Case 1 (Nozzle diameter)	12.7 mm	5.816e+02	1.115
	20.2 mm	5.464e+02	1.048
Case 2 (Molecular weight)	Hydrogen	5.660e+02	1.085
	Helium	6.924e+02	1.327
Case 3 (Steam fraction)	0.25	5.195e+02	0.996
	0.50	5.608e+02	1.075
	0.75	6.659e+02	1.276
	0.95	3.548e+04	68.00

RCR* (Reference case to various Case Ratio) = DF for each case/reference case.

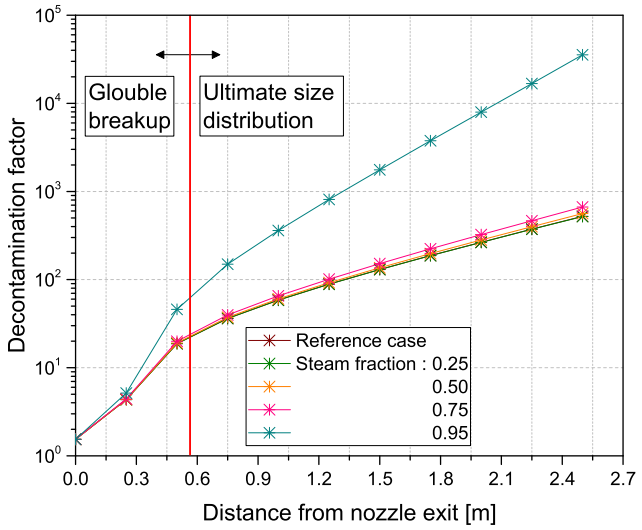

Fig. 8. Comparison of the decontamination factors for various steam fractions in the carrier gases.

equivalent diameters decrease rapidly when the steam fractions are higher than 0.95 since most steam condenses before the globule completely breaks up into small bubbles as explained in Section 2. From the sensitivity studies in this Section, we can conclude that the steam fraction is one of the most important factors in the calculation of the bubble-size-dependent decontamination factors.

5. Application of I-COSTA to numerical analyses on LACE-ESPAÑA experiments

5.1. Experimental conditions of LACE-ESPAÑA and computation conditions of I-COSTA

In this Section, we apply I-COSTA to analyses of the LACE-ESPAÑA experiments to validate the calculational method for the bubble-size-dependent decontamination factors. Among the various tests in the LACE-ESPAÑA experiments, we compare the tests listed in Table 8, which are performed using a single nozzle with a globular regime; i.e., the Weber number at the nozzle exit of the experiments is less than 1E+05. In the experiments, CsI aerosol particles are used. The size of the aerosol particles is various depending on the tests. Information on the aerosol particles is provided in Table 7. Geometrical conditions for the various tests are the same as listed in Table 4 and thermophysical conditions of the various tests are presented in Table 8.

The size distribution of the aerosol particles is divided into 10 discretized sections. The region between the nozzle exit and the top of the pool where the globule and the bubbles rise is divided into 10 sub-regions. The length of each sub-region is 25 cm. For sensitivity studies on the number of discretized sections of the bubbles, we consider two cases: one with seven discretized sections and the other with 15 discretized sections. Note that the number of discretized sections in the bubble size distribution is determined by the sensitivity studies on the decontamination factors, as discussed in Section 3 [29].

Table 7
Information of the aerosol particles used in the various LACE-ESPAÑA experiments.

Tests	AMMD[a] [cm]	GSD[b]	Steam fraction
RT-SB-00/01	3.4E-04	2.6	0.90
RT-SB-02/03	5.0E-04	3.8	0.87
RT-SB-04/05	3.4E-04	5.4	0.58
RT-SB-06/07	4.2E-04	3.3	0.56
RT-SB-08/09	5.5E-05	1.6	0.38
RT-SB-10/11	7.2E-04	1.6	0.35
RT-SB-12/13	3.0E-04	2.3	0.11
RT-SB-14/15	5.8E-04	3.5	0.15

[a] AMMD: Aerodynamic mass median diameter.
[b] GSD: Geometric standard deviation.

5.2. Comparison of the numerical results with those by SPARC-90 and experimental results

The numerical results are compared to the numerical results of SPARC-90 as well as to the experimental results. In the case of calculations by SPARC-90, we consider two cases: one with default sensitivity coefficients on the average equivalent diameter of the bubbles (Default), and the other using the average equivalent diameter, which is obtained from averaging the bubble size distributions in EPRI experiments (MD); i.e., the average equivalent diameter is the same as that used in I-COSTA. Modification of the average equivalent diameter of the bubble is done by changing the sensitivity coefficients on the bubble size. Note that both cases on SPARC-90 do not consider the size distribution of the bubbles. Instead, they use a SINGLE value for the average bubble equivalent diameter. Comparison of the numerical results obtained by the latter case of SPARC-90 calculations to those obtained by I-COSTA can show the effect of size distributions of the bubbles in the calculation of the decontamination factors. Computational conditions of the numerical analyses are summarized in Table 9. The numerical values of the decontamination factors are compared in Table 10 and Fig. 9.

As shown in Table 10 and Fig. 9, for most of the results on the analyses, I-COSTA shows that the decontamination factors are within the range of uncertainty in the tests. However, the decontamination factors, obtained by SPARC-90 with default sensitivity coefficients, are much lower than the experimental results, i.e., 3.7 times lower than the experimental results for the RT-SB-06/07 test. The results are attributed to SPARC-90 employing conservative calculations in the decontamination factor; i.e., the average equivalent diameter of the bubble in SPARC-90 is ~0.7 cm, which may give 32.5 times lower net deposition velocity, as shown in Section 4.1.

The results of SPACR-90 with the average equivalent diameter obtained from the size distribution of the bubbles considered in I-COSTA give enhanced decontamination factors compared to the results of SPAC-90 with default sensitivity coefficients; i.e., the decontamination factor for the RT-SB-06/07 by SPARC-90 is 1.85 times lower than the experimental results. However, compared to the results of I-COSTA and experimental results, the decontamination factors are still underestimated. The cause of the results is that the net velocity of the aerosol particles used to calculate the decontamination factors is not a simple linear function of the equivalent diameters of the bubbles. Instead, it increases dramatically as the equivalent diameter of the bubbles approaches zero, as shown in Fig. 3. The computing times of I-COSTA and those of SPARC-90 are compared in Table 11. Even though the computing time of I-COSTA is two times longer than that of SPARC-90, the order of computing times is around 1E-02 s. Therefore, it would not be a huge burden when we calculate the bubble-size-dependent decontamination factors coupled with severe accident analysis codes such as MELCOR [12], ASTEC [31], COCOSYS [32], THALES [33], etc.

5.3. Importance of the decontamination factors during pool scrubbing

We also analyze the importance of decontamination factors for

Table 8
Thermophysical conditions of the various tests in LACE-ESPAÑA experiments.

Tests	Carrier gas		Pool		Volumetric flow rate[m^3/sec]
	Pressure[Bar]	Temperature[K]	Pressure[Bar]	Temperature[K]	
RT-SB-00/01	2.29	413.55	1.99	383.45	7.700E-05
RT-SB-02/03	2.37	413.95	1.98	382.85	1.074E-04
RT-SB-04/05	2.29	437.85	1.91	382.75	3.024E-04
RT-SB-06/07	2.41	430.85	1.96	383.25	3.051E-04
RT-SB-08/09	2.30	426.15	2.00	382.55	3.019E-04
RT-SB-10/11	2.40	397.25	1.90	385.55	4.558E-04
RT-SB-12/13	2.28	423.15	1.98	382.65	6.727E-04
RT-SB-14/15	2.38	418.05	1.98	382.65	6.224E-04

Table 9
Computational conditions of the analyses for LACE-ESPAÑA experiments.

Parameters	SPARC-90		I-COSTA	
	Default	MD[a]	7	15
Number of sub-regions for globule and bubble rise	10	10	10	10
Number of sections for **aerosol particles**	10	10	10	10
Number of sections for **bubbles**	1	1	7	15

[a] MD: SPARC-90 using the average equivalent diameters which are obtained from averaging the bubble size distributions in EPRI experiments.

Table 10
Comparison of calculate-to-experimental (CE) ratio of the decontamination factors for SPARC-90 and I-COSTA.

Tests	Exp. DF	SPARC-90		I-COSTA	
	min.-max	Default	MD	7	15
RT-SB-00/01	129–254	0.52	0.65	1.06	0.96
RT-SB-02/03	567–922	0.36	0.76	1.20	1.03
RT-SB-04/05	168–169	0.45	0.74	1.04	0.95
RT-SB-06/07	419–858	0.27	0.54	0.81	0.72
RT-SB-08/09	16–20	0.51	0.66	1.11	0.94
RT-SB-10/11	677	0.47	0.74	1.10	0.97
RT-SB-12/13	444–702	0.37	0.60	1.01	0.84
RT-SB-14/15	52–53	0.71	0.885	1.07	0.97

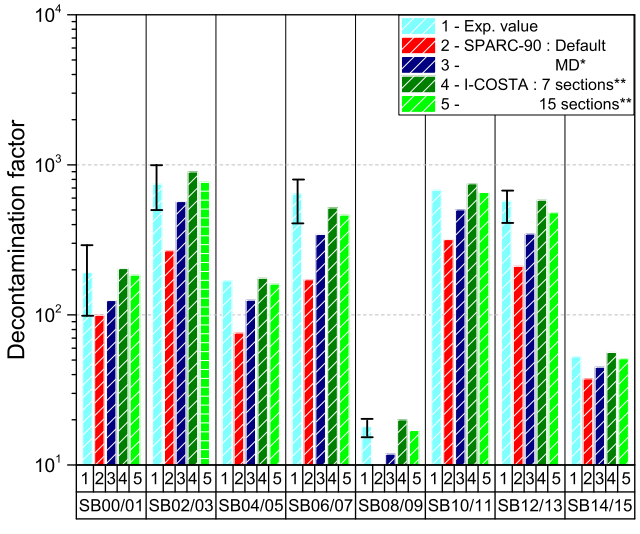

Fig. 9. Comparison of the decontamination factors for various LACE-ESPAÑA experiments.

each zone of the pool scrubbing in order to emphasize the necessity of bubble size distribution during the pool scrubbing. In the analyses, the length of the transition zone is defined by the distance between the point where the initial globule is located and the point where the critical Weber number of the globule is 15. The importance in the analyses is defined by Eq. (25) such that the summation of the importance for all regions is 1. The importance for the various tests of the LACE-ESPAÑA is shown in Fig. 10.

$$IMP_k = \frac{\log(DF_k)}{\sum_k \log(DF_k)}, \tag{25}$$

where k is the zone index (injection zone, transition zone, and bubble rise zone).

As shown in Fig. 10, the importance of the transition zone is not negligible. The difference in importance between the transition

Table 11
Comparison of computing time [sec] of I-COSTA and SPARC-90 for analyses of LACE-ESPAÑA experiments.

Tests	SPARC-90		I-COSTA	
	Default	MD	7	15
RT-SB-00/01	1.5E-02	1.5E-02	4.6E-02	9.3E-02
RT-SB-02/03	3.1E-02	3.1E-02	3.1E-02	7.8E-02
RT-SB-04/05	1.5E-02	1.5E-02	7.8E-02	9.4E-02
RT-SB-06/07	4.6E-02	4.6E-02	6.2E-02	7.8E-02
RT-SB-08/09	3.1E-02	3.1E-02	1.1E-01	2.0E-01
RT-SB-10/11	3.1E-02	3.1E-02	4.6E-02	9.3E-02
RT-SB-12/13	3.1E-02	3.1E-02	7.7E-02	7.8E-02
RT-SB-14/15	2.9E-02	2.9E-02	4.7E-02	7.8E-02

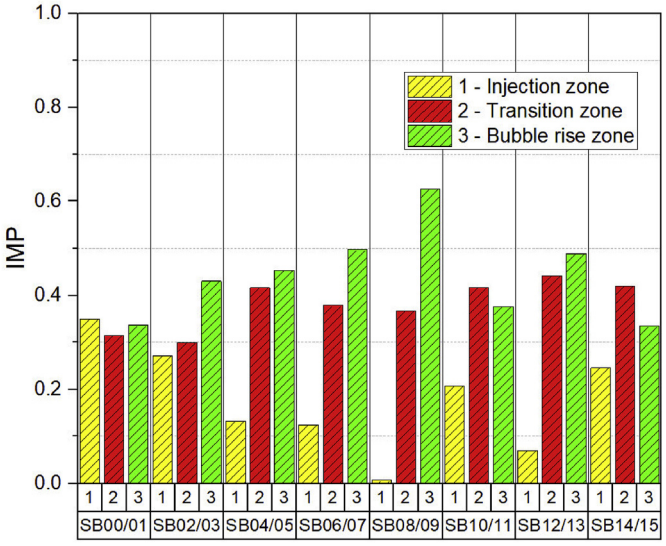

Fig. 10. Importance of the decontamination factors for each zone of pool scrubbing.

Table 12
Volume fraction of bubbles in transition zone for the various LACE-ESPAÑA experiments calculated by I-COSTA and SPARC-90.

Tests	Fraction of bubbles
RT-SB-00/01	0.9738
RT-SB-02/03	0.9454
RT-SB-04/05	0.8338
RT-SB-06/07	0.8301
RT-SB-08/09	0.7979
RT-SB-10/11	0.7220
RT-SB-12/13	0.7376
RT-SB-14/15	0.7441

zone and the bubble rise zone when the ultimate size distribution is achieved is within 2% for RT-SB-00/01. The cause of the results is that, as shown in Table 12, the volume fraction of the bubbles in the transition zone is significant and consequently there is noticeable retention of aerosol particles in this zone. Therefore, it is necessary to measure the size distributions of the bubbles in the transition zone to consider the retention of the aerosol particles in the transition zone more realistically. Note that, in this study, we assume that the size distributions of the bubbles remain static for the entire region where the globule and the bubbles rise due to a lack of information on the size distribution of the bubbles.

6. Conclusions and future work

In this study, we proposed a calculational procedure for the decontamination factors in pool scrubbing considering the size distributions of the bubbles obtained from EPRI experiments. We then performed sensitivity analyses on the deposition mechanisms of the aerosol particles with the various size distributions and also performed analyses on the various size distributions of the bubbles. In the case of analyses on the deposition mechanism, we considered typical sizes of the aerosol particles during a severe accident as the sizes of the aerosol particles during the pool scrubbing. Among the various mechanisms of the deposition, for the size of aerosol particles produced during severe accidents, we found that centrifugal deposition is the most dominant mechanism during pool scrubbing. We also found that it is the most sensitive to the bubble equivalent diameter. In the case of the sensitivity analyses on the size distributions of the bubbles, we found that the steam fraction is the most sensitive factor in the calculation of the bubble-size-dependent decontamination factors.

With the implementation of the aforementioned calculational procedure for the decontamination factors in I-COSTA, we performed analyses of the LACE-ESPAÑA experiments and compared the numerical results of I-COSTA to those of SPARC-90 as well as to the experimental results. The decontamination factors obtained from I-COSTA were within the uncertainty range of the experiments. However, SPARC-90 with default sensitivity coefficients showed much lower decontamination factors than those of the experiments. The results are attributed to SPARC-90 employing a conservative calculation in the decontamination factor as discussed earlier part in this paper. Even though the average equivalent diameter of bubbles is equal to that in I-COSTA, decontamination factors were still underestimated.

In the case of computing time, even though I-COSTA shows two times longer computing time for the most cases considered in this study, it is within the order of 1E-02 s. Therefore, it would not be a huge burden when we calculate the decontamination factors coupled with severe accident codes.

From the analyses on the importance of the decontamination factors during pool scrubbing, we found that the importance of decontamination factors in the transition zone is not negligible compared to those in the bubble rise zone where the ultimate size distributions of the bubbles are achieved. Therefore, for a more realistic evaluation of the decontamination factors, it is necessary to perform experiments to measure the size distributions of the bubbles in the transition zone.

The recent nuclear accident at three of the Japanese Fukushima Daiichi reactors following the devastating 2011 earthquake and tsunami sparked renewed interest in the development and validation on the current modeling of the pool scrubbing, by international cooperative research projects, such as IPRESCA by EU-NUGENIA [3], ARC-F by Nuclear Energy Agency (NEA) [4], etc. With the aforementioned interest, computer codes for the pool scrubbing should be extended to analyze the phenomena occurring at the jet injection regime, where the Weber number of the carrier gas at the nozzle exit is higher than 1E+05. For analyses at the jet injection regime, I-COSTA could be enhanced with the results of previous work carried out by some of the authors [34], which is based on the work by Berna et al. [35]. Note that most of the conventional computer codes have been developed to analyze pool scrubbing at the globular regime as discussed in the previous Sections.

In this study, the local surface velocity of the bubble, i.e., Eq. (4), is derived by assuming the internal flow of the bubble as static potential energy. According to Ref. [36], however, surface deformation of the bubble is not negligible in the range of Reynolds and Weber numbers for the bubbles of interest in this study, which results in a change of the aspect ratio of the bubbles. Such effect will be studied as future work.

During a severe accident, the water in the nuclear power plant would be contaminated by various impurities if we consider that sea water is used in the extreme condition during severe accident management. This contaminated water can also affect the pool scrubbing by causing the bubble rise velocities [30] to be slower than those in pure water, as discussed in the previous section, which results in slower centrifugal deposition velocities. In addition, the contaminated water shows physical and chemical characteristics different from those of pure water, e.g., surface tension, viscosity, etc. Such differences would lead to different size distributions of the bubbles. These effects should also be studied in order to perform analyses on pool scrubbing more realistically.

We will also extend the method to pool scrubbing of gaseous form of iodine, which is also important for evaluation and mitigation of the source term during a severe accident. The aforementioned future work will facilitate both understanding and evaluation of pool scrubbing behaviors in the analyses of severe accidents.

Declaration of competing interest

The authors declare that they have no known competing financial interests or personal relationships that could have appeared to influence the work reported in this paper.

Acknowledgements

This work was supported by the Nuclear Safety Research Program through the Korea Foundation Of Nuclear Safety (KoFONS) using financial resources granted by the Nuclear Safety and Security Commission (NSSC) of the Republic of Korea (No. 1805001).

Appendix A. Supplementary data

Supplementary data to this article can be found online at https://doi.org/10.1016/j.net.2020.08.013.

References

[1] H.-J. Allein, A. Auviene, J. Ball, S. Güntay, L. Herranz, A. Hidaka, A. Jones, M. Kissane, D. Power, G. Weber, State-of-the-art Report on Nuclear Aerosol, Organisation for Economic Co-operation and Development (OECD) Nuclear Energy Agency (NEA), Boulogne-Billancourt, France, 2009, p. 5. NEA/CSNI/R(2009.

[2] D.A. Powers, J.E. Brockmann, A.W. Shiver, VANESA : A Mechanistic Model of Radionuclide Release and Aerosol Generation during Core Debris Interactions with Concrete, Sandia National Laboratories, Albuquerque, NM, 1986. NUREG/CR-4308, SAND85-1370.

[3] S. Gupta, Main insights and perspectives of pool scrubbing research: examples of Thai and NUGENIA/IPRESCA, In : PASSAM Final Workshop on Source Term Mitigation of Severe Accidents, Paris, France, February 28- March 1, 2017.

[4] M. Yu, Program of work and overall work steps of ARC-F project, In : The First Meeting of PRG of the OECD/NEA ARC-F Project, Boulogne-Billancourt, France, January 22-23, 2019.

[5] M. Escudero, M.J. Marcos, M. Swiderska-Kowalczyk, M. Martin, J. López, State-of-the-art review on fission products aerosol pool scrubbing under severe accident conditions, in: Nuclear Science and Technology, European Commission Report EUR 16241 En. Official Publications of the European Communities ECSC-EC-EAEC, Brussels, Belgium, 1995.

[6] L.E. Herranz, M.J. Escudero, V. Peyrés, J. Polo, J. López, Review and Assessment of Pool Scrubbing Models, CIEMAT, Madrid, Spain, 1996. ISSN 1135-9420.

[7] A.T. Wassel, A.F. Mills, D.C. Bugby, Analysis of radionuclide retention in water pools, Nucl. Eng. Des. 90 (1985) 87–104.

[8] D.D. Paul, L.J. Flanigan, R.A. Cudnik, J.C. Cunnane, R.P. Coller, Radionuclide Scrubbing in Water Pools Volume 1 : Gas-Liquid Hydrodynamics, Electric Power Research Institute, Palo Alto, CA, 1985. NP-4154.

[9] D.D. Paul, L.J. Flanigan, R.A. Cudnik, J.C. Cunnane, R.P. Coller, Radionuclide Scrubbing in Water Pools Volume 2 : Gas-Liquid Hydrodynamics with Full-Scale Downcomer and Horizontal Vent, Electric Power Research Institute, Palo Alto, CA, 1991. NP-4154.

[10] P.C. Owczarski, K.W. Burk, SPARC-90: A Code for Calculating Fission Product Capture in Suppression Pools, U.S. Nuclear Regulatory Commission, Washington, DC., USA, 1991. NUREG/CR-5765, TI92 003256.

[11] S.A. Ramsdale, S. Guentay, H.G. Friederichs, BUSCA-JUN91 Reference Manual, Paul Scherrer Institut, Villigen, Switzerland, 1995. PSI Bericht Nr. 95-05.

[12] R.O. Gauntt, et al., MELCOR Computer Code Manuals Vol. 2: Reference Manual, Version 1.8.6, Sandia National Laboratories, Albuquerque, NM, USA, 2001. NUREG/CR-6119.

[13] M.J. Marcos, F.J. Gómez, I. Melches, M. Martín, J. López, LACE-ESPAÑA Experimental Programme on the Retention of Aerosols in Water Pool, Final Reports, CIEMAT, Madrid, Spain, 1994. ITN/TS-08/DP-93.

[14] A. Dehbi, D. Suckow, S. Guentay, Aerosol retention in low-subcooling pools under realistic accident conditions, Nucl. Eng. Des. 203 (2001) 229–241.

[15] T. Albiol, L. Herranz, E. Riera, C. Dailbart, T. Lind, A. Del Corno, T. Kärkelä, N. Losch, B. Azambre, C. Mun, L. Cantrel, Main results of the European PASSAM project on severe accident source term mitigation, Ann. Nucl. Energy 116 (2018) 42–56.

[16] Nuclear safety act in Korea, Accessed on, https://elaw.klri.re.kr/kor_mobile/viewer.do?hseq=45486&type=sogan&key=61, 2017. (Accessed 3 June 2020).

[17] Y. Lee, Y. J. Cho, and S. Lee, Results on benchmark problems for bubble hydrodynamics & preliminary sensitivity studies on size distribution of bubbles to decontamination factor via I-COSTA, In : 3rd Meeting of the IPRESCA Project, Frankfurt, Germany, June 27-28, 2019.

[18] P.H. Calderback, A.C. Lochiel, Mass transfer coefficients, velocities and shapes of carbon dioxide bubbles in free rise through distilled water, Chem. Eng. Sci. 19 (1964) 485–503.

[19] N. Zuber, J.A. Findlay, Average volumetric concentration in two-phase flow system, J. Heat Tran. 87 (1965) 453–468.

[20] W.L. Haberman, R.K. Morton, Experimental Investigation of the Drag and Shape of Air Bubbles Rising in Various Liquid, David Taylor Model Basin Report, Carderlock, MD, 1953. DTMB No. 802, 55715-102.

[21] N.H. Fuch, The Mechanics of Aerosols, The Macmillan Company, New York, 1964.

[22] R.B. Bird, W.E. Stewart, N.E. Lightfoot, Transport Phenomena, second ed., John Wiley and Sons, Inc., New York, 2007.

[23] J. Crank, The Mathematics of Diffusion, Oxford University Press, London, England, 1967.

[24] H.R. Pruppacher, J.D. Klett, Microphysics of Clouds and Precipitation, D. Reidel Publishing Co., Dordrecht, Holland, 1980.

[25] K. Eckerman, J. Harrison, H.-G. Menzel, C.H. Clement, ICRP Publication 119 – Compendium of Dose Coefficients Based on ICRP Publication 60, Elsevier, Oxford, UK, 2012. ISSN 0146–6453.

[26] T. Haste, F. Payot, P.D.W. Bottomley, Transport and deposition in the Phébus FP circuit, Ann. Nucl. Energy 61 (2013) 102–121.

[27] M. Laurie, P. March, B. Simondi-Teisserie, F. Payot, Reprint of "containment behavior in phébus FP, Ann. Nucl. Energy 61 (2013) 122–134.

[28] M.Y. Kim, Y.S. Bang, T.K. Park, D.Y. Lee, B.C. Lee, S.H. Park, Containment aerosol characterization during nuclear power plant severe accident, Part. Sci. Technol. 34 (2016) 622–632.

[29] Y. Lee, et al., Implementation of Calculational Procedure for Bubble-size-dependent Decontamination Factors in Pool Scrubbing, Korea Institute of Nuclear Safety, Daejeon, Korea, 2019. KINS/RR-1959 (Internal report written in Korean).

[30] S.H. Park, C. Park, J. Lee, B. Lee, A simple parameterization for the rising velocity of bubbles in a liquid pool, Nucl. Eng. Technol. 49 (2017) 692–699.

[31] J. Bestele, W. Klein-Heβling, ASTEC V0- CPA-module Containment Thermal Hydraulics and Aerosol- and Fission Product Behaviour– User Guideline, Gesellschaft fûr Anlagen– und Reaktorsicherheit (GRS)mbH, Germany, 2000. ASTECV0/DOC/00-14.

[32] W. Klein-Heβling, et al., COCOSYS V1.2 User Manual, Gesellschaft fûr Anlagen– und Reaktorsicherheit, GRS)mbH, Germany, 2000. GRS-P-3.

[33] M. Kajimoto, et al., Development of THALES-2, A computer code for coupled thermal hydraulics and FP transport analyses for severe accident at LWRs and its application to analysis of FP revaporization phenomena, in: Proc. Int. Topical Mtg. On Safety of Thermal Reactors, 1991. Portland, OR, USA, July 21-25.

[34] Y. Lee, Y.J. Cho, Sensitivity studies of entrained droplet concentrations on pool scrubbing in jet injection regime, in: The Eleventh Korea-Japan Symposium on Nuclear Thermal Hydraulics and Safety (NTHAS-11), 2018. Busan, Korea, November 18-21.

[35] C. Berna, A. Escrivá, J.L. Muñoz-Cobo, L.E. Herranz, Enhancement of the SPARC90 code to pool scrubbing events under jet injection regime, Nucl. Eng. Des. 300 (2016) 563–577.

[36] R. Clift, J.R. Grace, M.E. Weber, Bubbles, Drops and Particles, Academic press, Inc., New York, 1978.